Acta Chim. Slov. **2017**, *64*, 479–490

Scientific paper

Functionalization of Graphene Oxide with 9-aminoanthracene for the Adsorptive Removal of Persistent Aromatic Pollutants from Aqueous Solution

Ali Balati,[1] Mohammad Ghanbari,[2] Sara Karimi Behzad[3] and Mostafa M. Amini*,[3]

[1] *Environmental Sciences Research Institute, Shahid Beheshti University, G.C., Tehran 1983963113, Iran*

[2] *Department of Organic Chemistry, Faculty of Chemistry, University of Kashan, Kashan, Iran.*

[3] *Department of Chemistry, Shahid Beheshti University, G.C., Tehran 1983963113, Iran*

* Corresponding author: E-mail: m-pouramini@sbu.ac.ir
Tel: +98-21-29903109; fax: +9-21-22431663

Abstract

A novel modified graphene oxide nanocomposite was fabricated via a facial procedure, aiming to removal of the aromatic pollutants from aqueous solution. The graphene oxide (GO) was functionalized with 9-aminoanthracene and produced graphene oxide-9-aminoanthracene (GO-9-AA). FTIR, XRD, TGA, TEM and Raman spectroscopy techniques were used for characterization of the adsorbents. Adsorption of naphthalene (NAP), acenaphthylene (ACN), and phenanthrene (PHN) as a model of polycyclic aromatic hydrocarbons (PAHs) was investigated by GO-9-AA. The adsorbent showed excellent removal efficiency towards PAHs from aqueous solution. Equilibrium data of the adsorption process were successfully fitted with Freundlich model from single solute system, and the maximum adsorption capacities followed the order of NAP > ACN > PHN. The kinetic analysis revealed that the overall adsorption process was fast and successfully fitted with the pseudo-second-order kinetic model. The anthracene ring makes GO-9-AA π-electron rich, thus facilitating π–π EDA interaction between NAP, ACN and PHN with GO-9-AA.

Keywords: Wastewater, Aromatic pollutant; Graphene oxide, PAHs

1. Introduction

Polycyclic aromatic hydrocarbons (PAHs) are a group of organic compounds that contain two or more fused rings of carbon and hydrogen. They are persistent environmental contaminants and usually arise from incomplete combustion of hydrocarbons and other organic materials such as petroleum, coal, gas, garbage, tobacco, wood, and biomass.[1,2] PAHs enter the environment from different sources, including combustion fuel gasses, wastewater, and runoff from the petroleum industry. They were identified in industrial and municipal wastewater, effluents, rain, surface and drinking water, soils, and plants.[3,4] PAHs can transport long distance in air and water due to their chemical persistence and semi-volatile na-

ture and are difficult to biodegrade. Presences of PAHs in the environment are of great concern because many of them are toxic, carcinogenic, and they tend to bioaccumulate in aquatic organisms. Some PAHs are capable of interacting with DNA to promote mutagenic and carcinogenic responses. Therefore, they are considered as priority pollutants by both the US Environmental Protection Agency (EPA) and the European Environmental Agency. So, efficient, low-cost and robust methods to decontaminate waters from PAHs are vital to protect human and environment. Numerous studies have focused on the effective elimination of PAHs from aqueous solutions by different strategies such as photocatalysis, adsorption, electrolysis, organobentonite, and sonication. Among these approaches, adsorption removal of PAHs has been considered as

an efficient technique due to its low-cost, high efficiency and facile operation routes. For the adsorptive removal of PAHs from aqueous environments, various kinds of adsorbents have been extensively investigated. However, the adsorption capacities of aforementioned materials are not sufficient. Therefore, it will be beneficial to develop new adsorbents with higher adsorption capacities for persistent organic pollutant management in the environment.

Carbon-based nanomaterials have unique π-electronic structure and been used as an excellent sorbents for the removal of aromatic compounds.[12–15] GO, as a newly found carbon-based nanomaterial with fascinating two-dimensional (2D) atomic structure and only one atomic thickness, have attracted considerable attention in a broad range of application in addressing environmental challenges.[16–18] Due to its large specific surface area (theoretical limit, 2630 m² g⁻¹), remarkable electronic properties and high ability of modification, potential environmental applications of GO as a superior adsorbent has been recognized for removal of organic and inorganic contaminants from water and gasses.[19,20] GO can be well-dispersed in water due to its abundant hydrophilic groups on its surface such as hydroxyl, carboxylic and epoxide.[21,22] In addition, the interaction between GO and pollutants is closely related to its surface structure which is tunable and flexible.[23,24] The surface of GO usually consists of two parts: unoxidized and oxidized zones. The unoxidized zone is referring to the lowly oxidized GOs while oxidized zones consist of both *sp³* zones and *sp²* clusters. The oxygen-containing functional groups could be found on the surface of GO in the oxidized zones. The *sp²* clusters are

affinitive to non-electrolytic organic compounds by π–π stacking or other hydrophobic interactions[26,27] whereas the oxygen-containing functional groups tend to bind hydrophilic species due to hydrogen bonding, ion exchange or coordination effects.[28,29] Due to diverse zones of GO with different adsorption affinity, the adsorption behavior of GO mainly depends on its surface structural feature. Therefore, introduction of a suitable functional group on GO surface can improve its adsorption capacity for the removal of target pollutants. In the current research GO was modified and functionalized with 9-aminoanthracene by formation of the chemical bonds between carboxyl groups of GO and amine groups of 9-aminoanthracene to produce GO-9-AA (Scheme 1). The aim of functionalization of GO with 9-aminoanthracene is to increase the *sp²* clusters in GO for enhancing adsorption of non-electrolytic organic compounds by π–π stacking or other hydrophobic interactions. The fabricated composite was utilized for the removal of NAP, ACN and PHN as a model of PAHs and adoption mechanism of aforementioned PAHs was also proposed. To the best of our knowledge, this research is the first example of GO-9-AA fabrication and its application for the removal of NAP, ACN and PHN from aqueous solution.
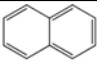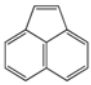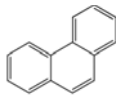
2. Experimental

2. 1. Materials

All reagents were the analytical grade and used without further purification. Graphite powder (~ 325 mesh si-
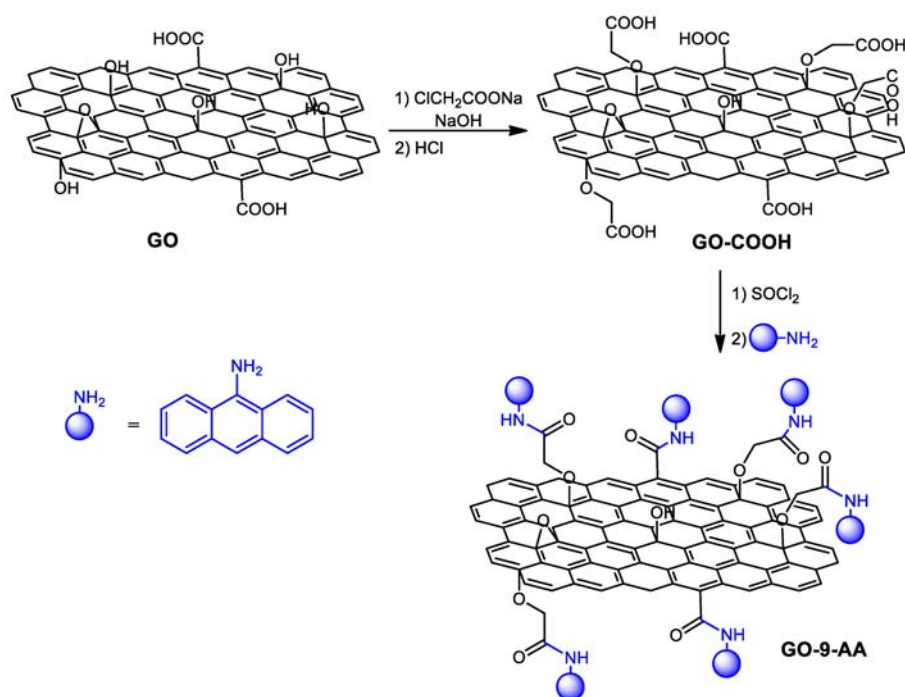
Scheme 1. Schematic illustration of GO-9-AA fabrication

Table 1. Physicochemical properties of the selected PAHs

PAH's	Structure	Molecular weight (g mol^{-1})	Vapour pressure at 25 °C Pa	Water solubility (g L^{-1})	log K$_{ow}$
Naphthalene C$_{10}$H$_8$		128	10.4	31~	3.37
Acenaphthylene C$_{12}$H$_8$		152	0.9	3.93	4.00
Phenanthrene C$_{14}$H$_{10}$		178	0.02	1.2	4.57

ze, 99.9995%) was obtained from Alpha Aesar Company (Karlsruhe, Germany). Sulfuric acid (H$_2$SO$_4$), potassium persulfate (K$_2$S$_2$O$_8$), phosphorus pentoxide (P$_2$O$_5$), potassium permanganate (KMnO$_4$), hydrogen peroxide (H$_2$O$_2$), hydrochloric acid HCl, hydrazine hydrate (H$_6$N$_2$O), nitric acid (HNO$_3$), glacial acetic acid, sodium hydroxide (NaOH) and SnCl$_2$ were purchased from Merck Chemical Company (Darmstadt, Germany). NAP, ACN, PHN and anthracene were purchased from Sigma-Aldrich Chemical Company (Dorset, UK). All aqueous solutions were prepared with ultrapure water (16 MΩ.cm) from the Milli-Q water purification system (Millipore, Bedford, MA, USA). The physicochemical properties of PAHs are shown in Table 1.

2. 1. 1. Fabrication of GO

GO was synthesized using modified Hummer's method. Graphite flakes were oxidized using a combination of powerful reagents, i.e., sulfuric acid (H$_2$SO$_4$), potassium persulfate (K$_2$S$_2$O$_8$) and phosphorus pentoxide (P$_2$O$_5$). Briefly, 3.0 g of graphite flakes were suspended in 10 mL of H$_2$SO$_4$. Oxidizing agents K$_2$S$_2$O$_8$ and P$_2$O$_5$ were gradually added to the graphite and sulfuric acid mixture and stirred at 90 °C until the flakes were dissolved. The stirring continued for 4 more hours at 80 °C, and the solution was then diluted with 500 ml Milli-Q Millipore water. After dilution, the solution was stirred overnight, and then filtered, washed with deionized water and thereafter dried to get the powdered form of GO. Pre-oxidized GO powder was then subjected to further oxidation with 125 mL of H$_2$SO$_4$ and 15 g of potassium permanganate (KMnO$_4$) in an ice bath. After 2 more hours stirring, 130 mL of Milli-Q Millipore water was added to the mixture, and this caused the temperature to rise to 95 °C. After 15 minutes, 15 mL hydrogen peroxide (30%, v/v) was added to reduce manganese to manganese sulfate (Mn → MnSO$_4$). Finally, the solution was diluted with 400 mL of Milli-Q Millipore water and yellowish suspension was stirred overnight. GO was filtered and washed thoroughly with HCl and water till the rinsed water pH was found to be approximately 7.

2. 1. 2. Preparation of 9-nitroanthracene (3)

9-nitroanthracene (**3**, Scheme 2) was prepared according to a previous report. Briefly, concentrated nitric acid (4 mL) was added dropwise to a suspension of anthracene (**1**) (10.0 g, 56.0 mmol) in glacial acetic acid (40 mL) maintaining the temperature below 30 °C. The reaction mixture was stirred vigorously for 1 h to form a clear solution. Then a mixture of concentrated HCl (50 mL) and glacial acetic acid (50 mL) was added slowly resulting in a pale yellow precipitate of 9-nitro-10-chloro-9,10-dihydroanthracene (**2**). The solution was filtered, and washed with glacial acetic acid (3 × 25 mL) and thoroughly with water until the washings were neutral. The resulting yellow solid was treated with a warm solution (60–70 °C) of 10% NaOH (200 mL), filtered, washed with warm water until the washings were neutral. Finally, the solid was air-dried and recrystallized from glacial acetic acid affording fluffy yellow needles (8.31 g, 67% yield), mp 148–150 °C (lit. 145–146 °C). R$_f$ = 0.30 (*n*-hexane/EtOAc 9:1). ^{1}H NMR (300 MHz, CDCl$_3$) δ = 8.57 (1H, s), 8.03 (2H, d, *J* = 7.6 Hz), 7.92 (2H, d, J = 7.6 Hz), 7.68–7.52 (4H, m).

2. 1. 3. Preparation of 9-aminoanthracene (4)

9-aminoanthracene (**4**, Scheme 2) was prepared according to the procedure reported by Janovec et al.,. Briefly, a suspension of 9-nitroanthracene (**3**) (7.24 g, 32.5 mmol) in glacial acetic acid (145 mL) was heated in 70–80 °C for 1.5 h. To the resulting clear solution was added a slurry of SnCl$_2$ (31.0 g, 163.2 mmol) in concentrated HCl (110 mL) via a dropping funnel. The resulting yellow precipitate was stirred at 80 °C for a further 30 min, cooled to room temperature, filtered, washed with concentrated HCl (3 × 10 mL), treated with a solution of 5% NaOH for approximately 15 min with manual stirring from time to time. Finally, product was collected by filtration, washed thoroughly with water until the washings were neutral and vacuum-dried at 50 °C for 6 h to afford a yellow powder (5.18 g, 83% yield). No further purification was required, M.p 161–166 °C (lit. 153–154 °C). R$_f$ =
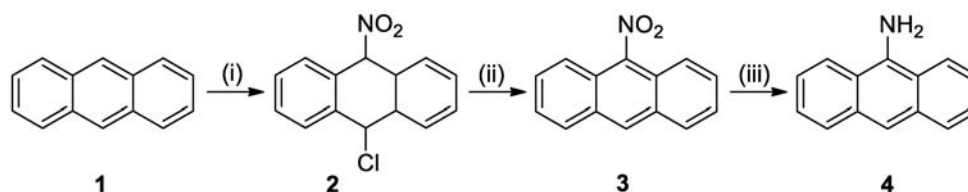
Scheme 2. Schematic illustration of 9-aminoanthracene synthesis. Reagents and conditions: (i) concd. HNO$_3$/HCl, <30 °C; (ii) NaOH (10%), 60–70 °C; (iii) SnCl$_2$/concd. HCl, glacial HOAc, 70–80 °C.

0.39 (*n*-hexane/EtOAc 3:1). ^{1}H NMR (300 MHz, CDCl$_3$): δ = 7.98-7.94 (m, 4H), 7.88 (s, 1H), 7.47–7.39 (m, 4H), 4.82 (s, 2H, NH$_2$).

2. 1. 4. Preparation of GO-9-AA

The GO suspension (1 mg/mL) was sonicated in the bath under 100W power for 1 h. The resulting suspension was taken for further carboxylation and amidation. In carboxylation of GO, 1.5 g NaOH and 1.5 g sodium chloroacetate were added into 300 mL GO suspension and sonicated in the bath for 1 h to convert hydroxyl and epoxide groups to carboxyl groups. The resulting mixture was neutralized with diluted HCl, and purified by repeated centrifugation at 4,000 rpm for 45 min and rinsed with ultrapure water, then evaporated to dryness in vacuum yielding a dark black solid product. The carboxylated graphene oxide, GO–COOH, was reacted in 20 mL of SOCl$_2$ (containing 2 mL of dimethylformamide) at 70 °C for 24 h to convert the carboxyl groups into acyl chlorides, then evaporated to dryness in the vacuum and resuspended in dry acetonitrile containing 9-aminoanthracene (500 mg). The mixture was stirred vigorously at 50 °C for 48 h under nitrogen atmosphere, and then the product was purified by repeated centrifugation at 4,000 rpm for 45 min and rinsed with ultrapure water, acetone, and dichloromethane to remove unreacted 9-aminoanthracene. The final product, graphene oxide-9-aminoanthracene (GO-9-AA), was dried at room temperature in vacuum yielding 270 mg.

2. 2. Characterization

The fabricated GO-9-AA was characterized by FTIR, XRD, TGA, TEM and Raman spectroscopy. FTIR spectra of materials were recorded within 400 to 4000 cm^{-1} region with Shimadzu FTIR 8300 spectrometer in KBr matrix. Raman spectra were measured using SENTERRA (2009) (BRUKER, Germany). The TGA data were acquired with Shimadzu TA-50 thermal analyzer (Shimadzu, Japan) at heating rate of 5 °C min^{-1} from room temperature to 800 °C. High-angle X-ray diffraction patterns were obtained with STOE diffractometer using Cu-Kα radiation at scanning rate of 3/min from 2θ = 5°–80°. The morphology of the GO-9-AA was recorded with Philips CM120 transmission electron microscopy (TEM).

2. 3. Batch Adsorption Experimental

All adsorption experiments were carried out in a batch reactor at 25 ± 1 °C. Different concentrations of NAP, ACN and PHN (1–30 mg L^{-1}) were made by preparation of simulated wastewater of three adsorbates (in pure methanol) with DI water. Adsorption experiments were conducted by adding a specific amount of GO-9-AA to the synthetic wastewater, including water/methanol solution (20% v/v) in 50 mL glass centrifuge tubes sealed with Teflon-lined screw caps. During the adsorption experiments, negligible amounts (0–0.15 μL) of 0.1 M HCl or 0.1 M NaOH were added to the solution for adjusting the pH to 7.0 ± 0.1. After obtaining the equilibrium, the mixture was centrifuged at 6000 rpm for 10 min, and then concentrations of the solutes in the supernatants phase were measured by UV/visible spectrophotometer (UV/Vis 2100 Shimadzu).

2. 4. Data Analysis

The equilibrium data of the adsorption experiments were fitted with two conventional isotherm models, i.e. Langmuir and Freundlich to determine the theoretical maximum adsorption capacity of the GO-9-AA. Based on the Langmuir isotherm model, adsorption process takes place on a homogeneous surface by monolayer adsorption, and there is no interaction between adsorbed particles. It is formulated as:

$$q_e = \frac{q_m b C_e}{1 + b C_e} \qquad (1)$$

Where C$_e$ is the equilibrium concentration of the adsorbate in mg L^{-1}, q$_e$ the amount of PAHs adsorbed at equilibrium in mg g^{-1}, q$_m$ and b are the Langmuir constants which demonstrate the adsorption capacity of adsorbent and apparent heat change in mg g^{-1} and l mg^{-1}, respectively.

Dimensionless constant separation factor (R$_L$) reflects the fundamental characteristics of Langmuir model, and it is expressed as:

$$R_L = \frac{1}{1 + b\, C_0} \qquad (2)$$

Where b is the Langmuir constant and C$_0$ is the highest initial concentration of adsorbate mg L^{-1}. The

value of R_L illustrates the types of Langmuir isotherm. Adsorption phenomenon is irreversible ($R_L = 0$), favorable ($0 < R_L < 1$), linear ($R_L = 1$), or unfavorable ($R_L > 1$). The Freundlich isotherm model assumes that adsorption process is multilayer and occurs on heterogeneous surfaces. The Freundlich isotherm model is given by:

$$q_e = K_F \, C_e^{1/n} \tag{3}$$

Where K_F ($mg^{(n-1)/n} \, g^{-1} \, L^{-1}$) and n are Freundlich isotherm model constants, representative of the saturation capacity and intensity of adsorption process.

The Kinetics of the adsorption of the NAP, ACN, and PHN onto GO-9-AA were investigated by fitting the adsorption data with pseudo first-order and pseudo-second-order kinetic models. The pseudo-first order assumes that adsorption rate is a proportion with the number of free adsorption sites and it is formulated as:

$$\log (q_e - q_t) = \log q_e - \frac{k_1}{2.303} t \tag{4}$$

Where q_e and q_t are the amounts of NAP, ACN and PHN adsorbed ($mg \, g^{-1}$) onto GO-9-AA at equilibrium and any time t (min), respectively, and k_1 is the rate constant of the adsorption process (min^{-1}).

The linear relationship between adsorption rate and the square of the number of unoccupied adsorption sites is an assumption of the pseudo-second order kinetic model, and it is given by:

$$\frac{t}{q_t} = \frac{1}{k_2 q_e^2} + \frac{t}{q_e} \tag{5}$$

Where k_2 is the adsorption rate constant ($mg \, g^{-1} \, min^{-1}$).

All of the isotherm and kinetic model parameters were obtained by fitting the models in Sigma Plot 12.0.

3. Results and Discussion

3. 1. Preparation of GO-9-AA

After modification of the GO surface by a chlorine group using thionyl chloride, the reaction of highly reactive chlorine with the amino group of 9-aminoanthracene is led to the formation of title sorbent. Pyridine was added to the reaction mixture to react with the side product (HCl). The formation of GO-9-AA nanocomposite was confirmed by IR spectroscopy, elemental analysis, thermal gravimetric analysis, Raman spectroscopy, powder X-ray diffraction and transmission electron microscopy.

3. 2. Characterization of GO-9-AA

3. 2. 1. FTIR Analysis

The FTIR spectra of GO and GO-9-AA are shown in Figure 1. The appearance of characteristic absorption peaks at 3449, 1735, 1631 and 1067 cm^{-1} revealed the stretching vibrations of –OH, C=O, C=C, and C–O functional groups in GO, respectively. After the amidation reaction, several new peaks appeared on the FTIR spectrum of GO-9-AA. The amide characteristic (–C(O)NH–) stretching vibration peak at 1653 cm^{-1} indicates that the amide bond formed by reaction between GO and 9-aminoanthrace. Furthermore, the new peak at 1573 cm^{-1} corresponds to the N–H bending vibration and the peak at 1192 cm^{-1} for C–N in-plane stretching demonstrates that the 9-aminoanthracene was grafted onto the GO by the amide bond.
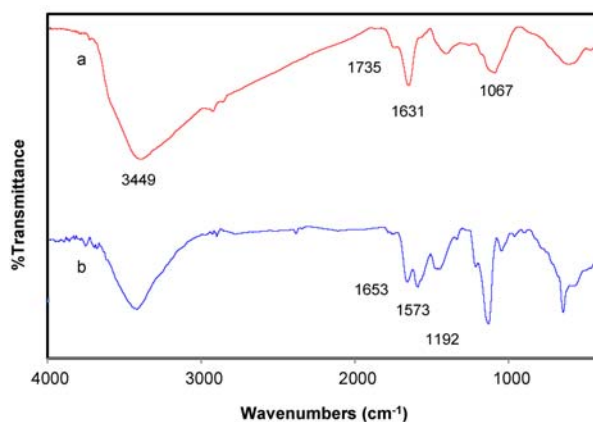

Fig. 1. FT-IR spectra of (a) GO and (b) GO-9-AA

3. 2. 2. Raman Spectroscopy

Raman spectroscopy as a powerful tool has been frequently used to investigate the structural and electronic
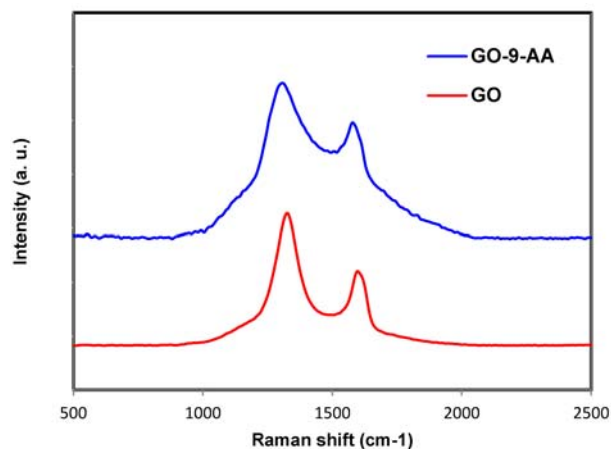

Fig. 2. Raman spectra of GO and GO-9-AA

properties of GO. Figure 2 shows the Raman spectra of the pristine GO and GO-9-AA. As expected, the pristine GO displays a prominent G-band (graphitic band) at 1598 cm^{-1} which is due to the influence of defects and isolated double bonds, and D-band (disorder band) at 1326 cm^{-1}. The D-band in carbon materials is associated with the presence of 'ždisorder' such as defects or simply nanoscale dimensions. The significant structural changes occurring during the amidation reaction were also reflected in the Raman spectra. In GO-9-AA, the G band shifts back to 1579 cm^{-1} which is relatively close to the G-band of the pristine graphite compared with GO, suggesting that electronic conjugation in GO-9-AA was restored after 9-aminoanthracene grafting on GO structure.[38,39]

3. 2. 3. TGA Analysis

Strong evidence for successful functionalization of the GO with 9-aminoantheracene was also provided via TGA analysis (Fig. 3). GO shows slight mass lose from room temperature to 210 °C and significant mass lose from 210 to 230 °C. Following with slight mass lose up to 600 °C. The major mass lose at ~ 220 °C is caused by pyrolysis of the oxygen-containing functional groups, generating CO, CO$_2$, and stream. In compared with GO, TGA of GO-9-AA shows an enhanced thermal stability due to the removal of oxygen-containing functional groups by amidation reaction. This change led to a new thermal decomposition at 490–570 °C which attributed to the formation of amide-bounds of 9-aminoanthracene functional group. This mass changes indicate successful covalent functionalization of GO by 9-aminoanthracene which was also in agreement with the results of FTIR and Raman analysis.
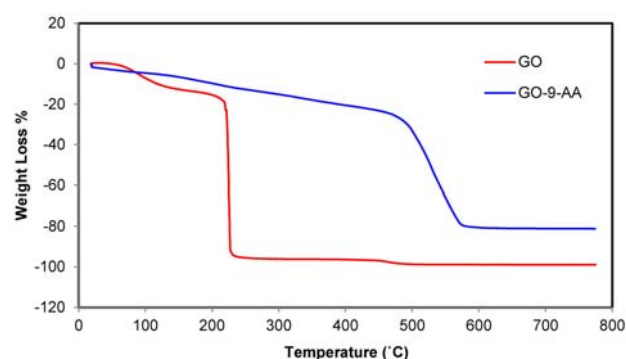

Fig. 3. TGA of GO and GO-9-AA

3. 2. 4. XRD Analysis

Figure 4 shows XRD patterns of both pristine GO and GO-9-AA. The peak at 11.06° corresponds to the (001) diffraction with an interlayer spacing of approximately 0.74 nm. As it can be seen, this peak in XRD pattern
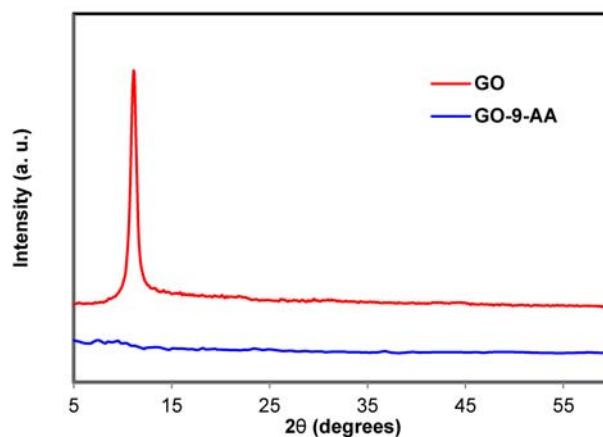

Fig. 4. X-ray diffraction patterns of GO and GO-9-AA

of GO after amidation has been eliminated, suggesting exfoliation of layered in GO-9-AA.

3. 2. 5. TEM Analysis

The natural structure of GO could be proved by natural ripples on the GO surfaces. The microstructure of the sorbent before and after modification was investigated by TEM analysis. The TEM images demonstrated that both GO and GO-9-AA nanosheets were transparent (Figure 5). As it can be seen, GO has fairly flat surface compared with that of GO-9-AA and its wrinkles were mainly positioned on the boundary regions of the GO and created scrolls, whereas the surface of GO-9-AA has more aggregations and wrinkles which mostly on the basal planes to make groove regions.

3. 3. Adsorption Isotherms

Describing the interaction between adsorbent and the adsorbate is usually the aim of adsorption isotherm models when the adsorption process reaches equilibrium. The isotherm models allow having the most vital parameter for designing an appropriate adsorption system. The adsorption isotherms of NAP, ACN, and PHN on GO-9-AA are shown in Figure 6, and the regression parameters are listed in Table 2. In general, all adsorption isotherms were nonlinear, and the regression parameters are listed in Table 2. The results indicated that the nonlinear correlation coefficients of the Freundlich isotherm model for NAP, ACN, and PHN onto GO were 0.991, 0.997 and 0.997, and onto GO-9-AA were 0.998, 0.997 and 0.997, respectively. The higher correlation coefficients for Freundlich model imply that adsorption process takes place mostly onto heterogeneous regions such as edges, grooves, and wrinkles. The same result has also been reported in the removal of PAHs by other adsorbent materials such as modified periodic mesoporous organosilica, GO and graphene.[45,46] Based on Langmuir isotherm mo-
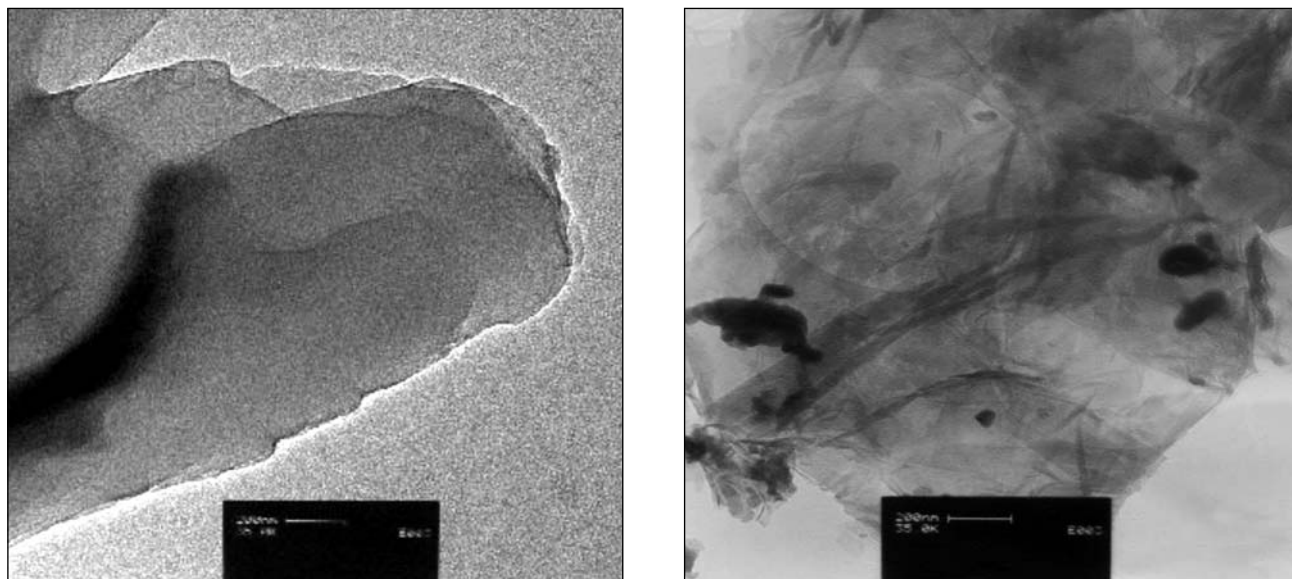
Fig. 5. TEM micrograph of GO (left) and GO-9-AA (right)

Table 2. Isotherm parameters for NAP, ACN, and PHN adsorption onto GO and GO-9-AA

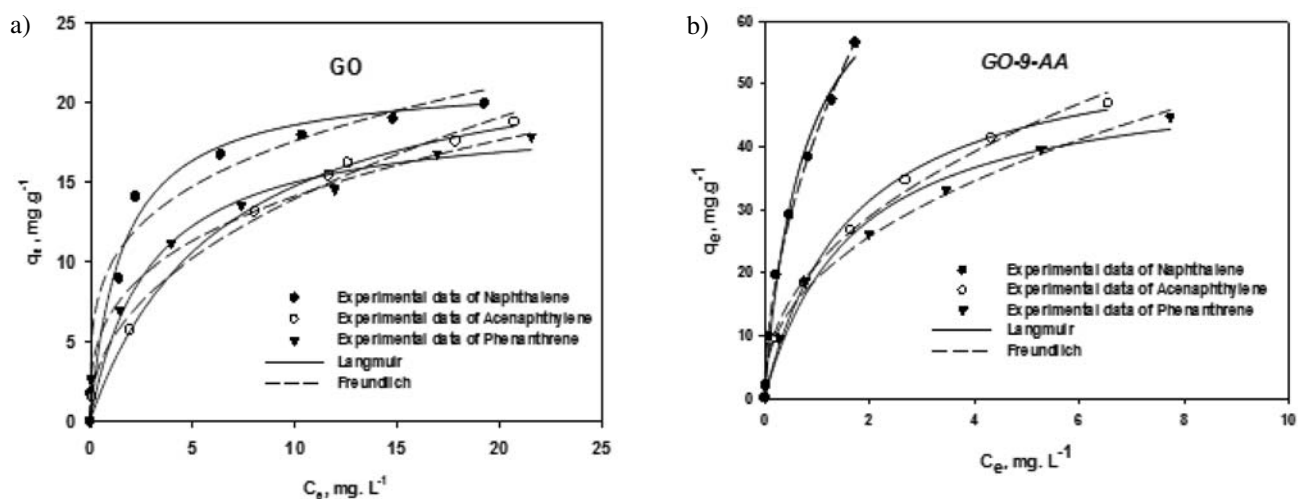|	Adsorbates	Langmuir					Freundlich		
		$q_{m,cal}$ (mg g^{-1})	$q_{e,exp}$ (mg g^{-1})	b (l mg^{-1})	R_L	R^2	Kf (mg$^{(n-1)/n}$ g^{-1} L^{-1})	N	R^2
GO	NAP	22.93	23.16	0.52	0.18	0.987	9.43	3.40	0.991
	ACN	18.80	21.28	0.38	0.21	0.995	4.93	2.22	0.997
	PHN	17.83	19.30	0.34	0.23	0.988	4.71	2.19	0.997
GO-9-AA	NAP	57.00	78.08	1.31	0.09	0.994	42.18	2.06	0.998
	ACN	46.32	57.60	0.59	0.16	0.995	21.18	2.26	0.997
	PHN	44.50	52.02	0.58	0.17	0.994	18.95	2.32	0.997

Fig. 6. Adsorption isotherms of NAP, ACN, and PHN onto GO and GO-9-AA at room temperature and pH =7.0

del, maximum theoretical adsorption capacity ($q_{m,cal}$) we-re obtained 23.16, 21.28 and 19.30 mg g^{-1} onto GO and 78.08, 57.60 and 52.02 mg g^{-1} onto GO-9-AA for NAP,

ACN, and PHN, respectively. The same trends were observed for experimental adsorption capacities ($q_{e,exp}$) i.e., 22.93, 18.80 and 17.83 mg g^{-1} for NAP, ACN and PHN

onto GO and 57.00, 46.33 and 44.50 mg g^{-1} onto GO-9-AA, respectively. Separation factor (R_L), derived from the Langmuir isotherm model was also calculated (Table 2) to prove the favorableness of the adsorption of three adsorbates onto GO and GO-9-AA. The values of R_L are calculated in the range of 0.09–0.23 demonstrating a favorable adsorption process of NAP, ACN, and PHN. Adsorption intensity of adsorbates could be attributed to the Freundlich constant (1/n). Adsorbates could be easily adsorbed when $0.1 < 1/n \leq 0.5$, adsorption process of the adsorbates is difficult when $0.5 < 1/n \leq 1$, and when $1/n > 1$ adsorption is entirely difficult to occur. The 1/n values of NAP, ACN, and PHN onto two adsorbents were calculated in the range of 0.1–0.5 proofing that the adsorbates could be easily adsorbed. Since GO-9-AA showed a notable adsorption capacity in comparison with GO, it was selected to precede extra adsorption experiments.

3. 4. Adsorption Kinetics

Rapid treatment of a large volume of drinking water is the main factor which sometimes limits practical application of the adsorbents. In order to investigate the required time for obtaining adsorption equilibrium, kinetic studies were performed. The effect of adsorption time on the removal of NAP, ACN, and PHN by GO-9-AA is shown in Figure 7. Adsorption kinetic data were evaluated with two
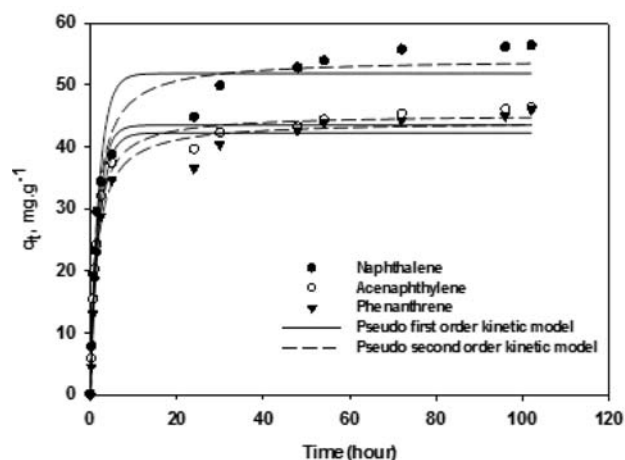

Fig. 7. Adsorption kinetics of NAP, ACN, and PHN on GO-9-AA at room temperature and pH =7.0.

semi-empirical kinetic models: the pseudo-first and second-order equations. The validity of two models was investigated by nonlinear regression. It can be seen from Figure 7, the adsorption rate was quite fast with the order of magnitude NAP > PHN > ACN within the first 20 h, and then gradually slowed down until equilibrium was reached within 48 h which quite similar to that reported for aromatic compounds. Parameters obtained with two models are summarized in Table 3. As depicted in Figure 7 and Table 3, predicted adsorption data of NAP, ACN, and PHN onto GO-9-AA by pseudo-second order kinetic model showed a quite good agreement with measured data for both fast and the slow adsorption steps (nonlinear correlation coefficients of the model for NAP, ACN, and PHN onto GO-9-AA were 0.991, 0.996 and 0.994, respectively). Constant rates of NAP, ANC, and PHN adsorption, in the liquid phase, are comparable to those calculated for other aromatic hydrocarbons on different adsorbents. The experimental values of q_e for NAP, ACN, and PHN were 56.3, 46.24 and 45.92 mg g^{-1}, respectively, which are consistent with the q_e values calculated from the pseudo-second order model which summarized in Table 3. The good agreement of adsorption kinetic data with pseudo-second order model indicates that adsorption of the target adsorbates on GO-9-AA is due to a chemical adsorption.

3. 5. Comparison of Adsorption Behavior Based on Literature Data

The efficacy of GO-9-AA adsorbent was evaluated in comparison with other adsorbents (Table 4). As it can be seen, the sorption capacity of PAHs on GO-9-AA composites is much higher than other adsorbents.

3. 6. Desorption

For the environmental protection and economic purposes, adsorbents should both have adequate capacity to decrease the pollutants concentration to satisfy environmental protection agencies standards and have been recycled and reused in successive cycles because they might have either precious raw substance or consist of hazardous materials. The recycling NAP, ACN, PHN and the regeneration of GO-9-AA are illustrated in Figure 8. The adsorption-desorption experiment results demonstrated that the efficiency of the applied GO-9-AA adsorbent

Table 3. Kinetic parameters of NAP, ACN, and PHN adsorption on GO-9-AA

Adsorbates		Pseudo-first-order			Pseudo-second-order		
		k_1 (min^{-1})	$q_{e,exp}$ (mg g^{-1})	R^2	$q_{e, cal}$	k_2(mg g^{-1} min^{-1})	$q_{e, cal}$ (mg g^{-1}) R^2
NAP	56.30	0.50	51.79	0.974	0.71	54.14	0.991
ACN	46.24	0.56	43.41	0.991	0.80	45.21	0.996
PHN	45.92	0.49	42.16	0.985	0.67	44.09	0.994

Table 4. Comparison of maximum adsorption capacity of different adsorbents for adsorption of PAHs

Adsorbent	Adsorbate	Adsorption capacity (mg.g^{-1})	Temperature (ºC)	Equilibrium Time (hour)	References
	NAP	1.63			
SBA-15-NH$_2$	ACN	1.01	25	10	[44]
	PHN	0.60			
PMO	NAP	46.64	28	50	[45]
RHAC	NAP	63.60	28	120	[46]
Activated carbon (Coconut Shell)	PHN	20.22	25	1	[47]
Multilayer Graphene	PHN	28.1	25	NA	[48]
MWCNT30	PHN	14.1	25	NA	[49]
Biochar	PHN	14	25	672	[50]
C60, Fullerene	NAP	2.3	25	72	[51]
Activated carbon	NAP	58.36	25	280	[52]
Zeolite	NAP	29.59	25	6	[53]
	NAP	78.08			
GO-9-AA	ACN	57.60	25	72	Present study
	PHN	52.02			

was satisfactory for the removal of target PAHs by removing 94% (56.50 mg g^{-1}), 79% (46.92 mg g^{-1}), and 74% (44.24 mg g^{-1}) of NAP, ACN, and PHN, respectively in the first cycle. As can be noticed on Figure 8, the absorption capacity of GO-9-AA remained essentially the same after five successive cycles of testing. After fifth adsorption-desorption experiments, the efficiency of GO-9-AA was 83.5% (50.09 mg g^{-1}), 68% (41.00 mg g^{-1}), and 66% (39.90 mg g^{-1}) of NAP, ACN, and PHN, respectively. The negligible decrease in the GO-9-AA capacity (around 10%) revealed the good reusability and stability of this adsorbent; therefore, it could be a suitable choice to be used efficiently for the treatment of wastewater polluted by PAHs.
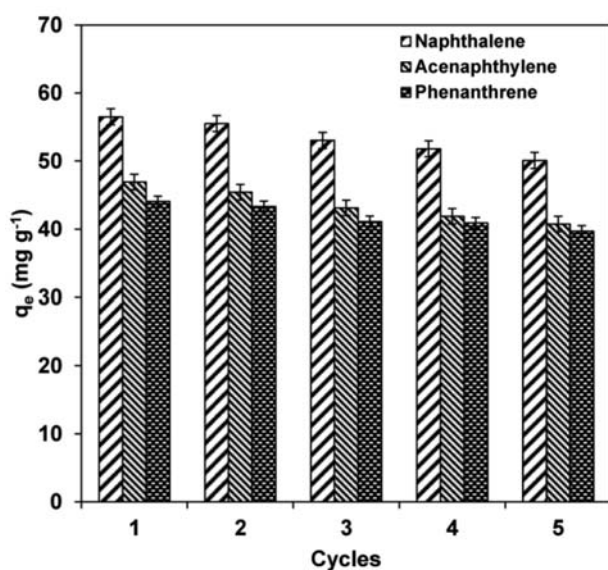
Fig. 8. Recycling of GO-9-AA in the adsorption of NAP, ACN, and PHN, at room temperature. and pH = 7.0

3. 7. Adsorption Mechanism

Isotherm and kinetic parameters of NAP, ACN, and PHN adsorption on GO-9-AA are listed in Table 2 and 3, respectively. As it can be seen, the maximum adsorption capacity (q_e) for three adsorbates are in the following order of magnitude NAP>ACN>PHN onto GO-9-AA. A similar behavior was also observed for the adsorption coefficient ($K_d = q_e/C_e$, in Fig.9) values at different equilibrium concentrations. As it depicted in Figure 9, adsorption coefficients for NAP, ACN, and PHN have a similar trend. However, a marked decrease in the K_d values for the three adsorbates (magnitude of decrease was in the order of NAP>ACN>PHN) was different. Based on the assumptions of Freundlich isotherm model, removal of NAP, ACN, and PHN by heterogeneous adsorption onto GO-9-AA is concerning to the presence of high surface energy sites, such as defects, edges, and groove areas.[60,61] In this case, three adsorbates would primarily be adsorbed with high affinities to these regions. Inherent surface heterogeneity on GO and increasing the amount of groove and folded regions of GO after functionalization (Figure 5) give rise to charge in homogeneities into the modified GO. Uneven charge sharing on the GO-9-AA could generate high active region in wrinkles and defect parts from the chemical perspective; as a result, NAP, ACN, and PHN could be adsorbed more in these active sites. As Figure 9 shows, adsorption coefficient values for three adsorbates reduce considerably with increasing concentrations, which is in agreement with the K_d-C_e curve obtained in the current study for GO-9-AA.

Figure 9 shows that the adsorption of three adsorbates is favorable at a low concentration. Also, the starting point and decreasing slope for NAP is larger than the other two adsorbates, i.e., ACN, and PHN which shows adsorption of NAP is more favorable than ACN, and PHN. Nevertheless, this is not consistent with the hydrophobi-
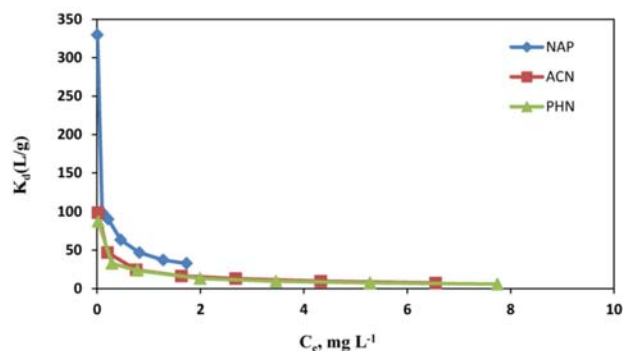
Fig. 9. Adsorption coefficients of NAP, ACN, and PHN onto GO-9-AA in different concentrations

city (K_{ow}) trend of the target PAHs, i.e., PHN>ACN>NAP. Wang and et al. suggested that different adsorption capacities of PAHs by carbonic adsorbents after eliminating hydrophobic effect might be due to sieving effect. Since adsorption of NAP, especially in the low concentration with approximately high solubility range is more favorable than ACN, and PHN; this shows more heterogeneous regions such as wrinkle surfaces, which have rich π-electron density onto GO-9-AA and readily available for the molecule with a smaller size.

Finally, several possible interactions between GO-9-AA and aromatic compounds (as an adsorbate) are responsible for the adsorption of NAP, ACN, and PHN. These interactions are a hydrophobic effect, electrostatic and electron donor-acceptor (EDA). Based on the adsorption mechanism between aromatic compounds and carbonaceous adsorbents[63] EDA interaction was proposed to be the main mechanism for adsorption of NAP, ACN, and PHN on GO-9-AA. One type of EDA interaction is π–π EDA interaction. π–π EDA interaction is specific and noncovalent, that exists between electron-rich and electron-poor compounds. The existence of anthracene rings on GO-9-AA makes it more electron-rich; therefore, the π–π EDA interactions between three adsorbates and GO-9-AA surface will be stronger and easier.

4. Conclusion

GO-9-AA composite was successfully prepared via a facial strategy, characterized and its performance evaluated for the removal of NAP, ACN, and PHN. Incorporation of 9-aminoanthracene in the structure of GO led to both high adsorption capacity and fast removal kinetics that was proved by isotherm and kinetic experiments. The adsorption isotherm and kinetic data were fitted better by Freundlich and pseudo-second-order, respectively. It seems that more conformational change of GO after functionalization with 9-aminoanthracene and stronger electron donor-acceptor interaction between NAP, ACN, and PHN with modified GO are the main reasons for higher

adsorption capacity of GO-9-AA for the removal of the target adsorbates. Furthermore, the adsorption efficacy of GO-9-AA was evaluated in comparison with other adsorbents. The results showed that the adsorption capacity of GO-9-AA for the removal of target PAHs is much higher than other adsorbents. Therefore, GO-9-AA could be considered as a promising adsorbent for the removal of PAHs from water in real world applications.

5. Acknowledgements

6. References

1. H. Guo, T. Jiao, Q. Zhang, W. Guo, Q. Peng and X. Yan, *Nanoscale Res. Lett.* **2015**, *10*, 272.
   https://doi.org/10.1186/s11671-015-0931-2
2. A. Balati, A. Shahbazi, M. M. Amini, S. H. Hashemi and K. Jadidi, *Eur. J. Environ. Sci.* **2014**, *4*.
3. D. P. Arfsten, D. J. Schaeffer and D. C. Mulveny, *cotoxicol. Environ. Saf.* **1996**, 33, 1–24.
   https://doi.org/10.1006/eesa.1996.0001
4. M. Maier, D. Maier and B. Lloyd, *Water Res* **2000**, 34, 773–786. https://doi.org/10.1016/S0043-1354(99)00230-4
5. X. Zhang, S. Xie, M. C. Paau, B. Zheng, H. Yuan, D. Xiao and M. M. F. Choi, *J. Chromatogr. A* **2012**, 1247, 1–9.
   https://doi.org/10.1016/j.chroma.2012.05.047
6. S.-S. Cai, J. A. Syage, K. A. Hanold and M. P. Balogh, *Anal. Chem* **2009**, 81, 2123–2128.
   https://doi.org/10.1021/ac802275e
7. Y. Ide, Y. Nakasato and M. Ogawa, *J. Am. Chem. Soc* **2010**, 132, 3601–3604. https://doi.org/10.1021/ja910591v
8. W. Chen, L. Duan, L. Wang and D. Zhu, *Environ. Sci. Technol* **2008**, 42, 6862–6868.
   https://doi.org/10.1021/es8013612
9. G. D. Sheng, D. D. Shao, X. M. Ren, X. Q. Wang, J. X. Li, Y. X. Chen and X. K. Wang, *J Hazard Mater* **2010**, 178, 505–516; https://doi.org/10.1016/j.jhazmat.2010.01.110
10. Y. Huang, A. N. Fulton and A. A. Keller, *Sci. Total Environ* **2016**, *571*, 1029–1036.
    https://doi.org/10.1016/j.scitotenv.2016.07.093
11. P. Zuman and J. Ludvík, *Electroanalysis* **2000**, 12, 879–888. https://doi.org/10.1002/1521-4109(200008)12:12<879::AID-ELAN879>3.0.CO;2-O
12. Z. Wu and L. Zhu, *J Environ Sci* **2012**, 24, 248–253.
    https://doi.org/10.1016/S1001-0742(11)60780-8
13. D. T. Sponza and R. Oztekin, *Chem. Eng. j.* **2010**, 162, 142–150. https://doi.org/10.1016/j.cej.2010.05.014
14. D. T. Sponza and R. Oztekin, *Bioresour Technol* **2010**, 101, 8639–8648.
    https://doi.org/10.1016/j.biortech.2010.06.124

15. S. Rengaraj, Y. Kim, C. K. Joo and J. Yi, *J. Colloid Interface Sci* **2004**, 273, 14–21.
https://doi.org/10.1016/j.jcis.2004.01.007

16. X. Luo, K. Ma, T. Jiao, R. Xing, L. Zhang, J. Zhou and B. Li, *Nanoscale Res. Lett* **2017**, *12*, 99.
https://doi.org/10.1186/s11671-017-1864-8

17. R. Xing, T. Jiao, Y. Liu, K. Ma, Q. Zou, G. Ma and X. Yan, *Polym. Sci.* **2016**, *8*, 181.

18. X. Zhao, K. Ma, T. Jiao, R. Xing, X. Ma, J. Hu, H. Huang, L. Zhang and X. Yan, *Sci. Rep* **2017**, *7*.

19. G. K. Ramesha, A. Vijaya Kumara, H. B. Muralidhara and S. Sampath, *J. Colloid Interface Sci* **2011**, 361, 270–27720.
https://doi.org/10.1016/j.jcis.2011.05.050

20. T. Jiao, Y. Liu, Y. Wu, Q. Zhang, X. Yan, F. Gao, A. J. Bauer, J. Liu, T. Zeng and B. Li, *Sci. Rep* **2015**, *5*, 12451.
https://doi.org/10.1038/srep12451

21. S. Park and R. S. Ruoff, *Nat. Nanotechnol* **2009**, 4, 217–224.
https://doi.org/10.1038/nnano.2009.58

22. M. J. Allen, V. C. Tung and R. B. Kaner, *Chem. Rev* **2009**, 110, 132–145. https://doi.org/10.1021/cr900070d

23. D. R. Dreyer, S. Park, C. W. Bielawski and R. S. Ruoff, *Chem. Soc. Rev* **2010**, 39, 228–240.
https://doi.org/10.1039/B917103G

24. X. Yuan, Y. Wang, J. Wang, C. Zhou, Q. Tang and X. Rao, *Chem. Eng. J.* **2013**, 221, 204–213.
https://doi.org/10.1016/j.cej.2013.01.090

25. Y.-B. Luo, J.-S. Cheng, Q. Ma, Y.-Q. Feng and J.-H. Li, *Anal. Methods* **2011**, 3, 92–98.
https://doi.org/10.1039/C0AY00624F

26. R. Kempaiah, S. Salgado, W. L. Chung and V. Maheshwari, *Chem. Commun.* **2011**, 47, 11480–11482.
https://doi.org/10.1039/c1cc15096k

27. C. Braun, C. Cook, C. Merritt and J. Rousseau, *ORG. SYNTH* **1951**, 31, 77–79.
https://doi.org/10.15227/orgsyn.031.0077

28. L. Janovec, G. Suchár, J. Imrich, P. Kristian, V. Sasinková, J. Alföldi and E. Sedlák, ***Collect***. ***Czech***. *Chem. Commun* **2002**, 67, 665–678.
https://doi.org/10.1135/cccc20020665

29. J. Sun, Z. Chen, M. Ge, L. Xu and M. Zhai, *J. Hazard. Mater.* **2013**, 244–245, 94–101.
https://doi.org/10.1016/j.jhazmat.2012.11.043

30. M. S. Morey, S. O'Brien, S. Schwarz and G. D. Stucky, *Chem. Mater* **2000**, 12, 898–911.
https://doi.org/10.1021/cm9901663

31. C. B. Vidal, A. L. Barros, C. P. Moura, A. C. A. de Lima, F. S. Dias, L. C. G. Vasconcellos, P. B. A. Fechine and R. F. Nascimento, *J. Colloid Interface Sci* **2011**, 357, 466–473.
https://doi.org/10.1016/j.jcis.2011.02.013

32. C. Namasivayam and D. Kavitha, *Dyes Pigm.* **2002**, 54, 47–58. https://doi.org/10.1016/S0143-7208(02)00025-6

33. J. Saikia, B. Saha and G. Das, *J. Hazard. Mater.* **2011**, 186, 575–582. https://doi.org/10.1016/j.jhazmat.2010.11.036

34. S. Sun, Y. Cao, J. Feng and P. Wu, *J. Mater. Chem. A* **2010**, 20, 5605–5607.

35. K. N. Kudin, B. Ozbas, H. C. Schniepp, R. K. Prud'Homme, I. A. Aksay and R. Car, *Nano Lett.* **2008**, 8, 36–41.
https://doi.org/10.1021/nl071822y

36. A. Lerf, H. He, M. Forster and J. Klinowski, *J. Phys. Chem. B* **1998**, 102, 4477–4482.
https://doi.org/10.1021/jp9731821

37. H.-K. Jeong, Y. P. Lee, R. J. Lahaye, M.-H. Park, K. H. An, I. J. Kim, C.-W. Yang, C. Y. Park, R. S. Ruoff and Y. H. Lee, *J. Am. Chem. Soc* **2008**, 130, 1362–1366.
https://doi.org/10.1021/ja076473o

38. A. Fasolino, J. Los and M. I. Katsnelson, *Nat. Mater* **2007**, 6, 858–861. https://doi.org/10.1038/nmat2011

39. O. Glukhova and M. Slepchenkov, *Nanoscale.* **2012**, 4, 3335–3344. https://doi.org/10.1039/c2nr30477e

40. Z. Pei, L. Li, L. Sun, S. Zhang, X.-q. Shan, S. Yang and B. Wen, *Carbon.* **2013**, 51, 156–163.
https://doi.org/10.1016/j.carbon.2012.08.024

41. J. Wang, Z. Chen and B. Chen, *Environ. Sci. Technol* **2014**, 48, 4817–4825. https://doi.org/10.1021/es405227u

42. L. N. Z. X.G. Luo, *J. Hazard. Mater* **2009**, 171, 340–347.
https://doi.org/10.1016/j.jhazmat.2009.06.009

43. X. Luo, C. Wang, L. Wang, F. Deng, S. Luo, X. Tu and C. Au, *Chem. Eng. J.* **2013**, 220, 98–106.
https://doi.org/10.1016/j.cej.2013.01.017

44. A. Balati, A. Shahbazi, M. M. Amini and S. H. Hashemi, *J water reuse desal.* **2015**, 5, 50–63.

45. C. B. Vidal, A. L. Barros, C. P. Moura, A. C. De Lima, F. S. Dias, L. C. Vasconcellos, P. B. Fechine and R. F. Nascimento, *J. Colloid Interface Sci* **2011**, 357, 466–473.
https://doi.org/10.1016/j.jcis.2011.02.013

46. S. Yakout, A. Daifullah and S. El-Reefy, *Adsorp. Sci. & Technol.* **2013**, 31, 293–302.
https://doi.org/10.1260/0263-6174.31.4.293

47. C. Zhang, X. Zhang, Z. Huang, D. Huang and Q. Cheng, *J Environ Anal Toxicol* **2012**, 2012.

48. J. Zhao, Z. Wang, Q. Zhao and B. Xing, *Environ. Sci. Technol* **2013**, 48, 331–339.
https://doi.org/10.1021/es403873r

49. K. Yang, L. Zhu and B. Xing, *Environ. Sci. Technol* **2006**, 40, 1855–1861. https://doi.org/10.1021/es052208w

50. T. H. Nguyen, H.-H. Cho, D. L. Poster and W. P. Ball, *Environ. Sci. Technol* **2007**, 41, 1212–1217.
https://doi.org/10.1021/es0617845

51. X. Cheng, A. T. Kan and M. B. Tomson, *J. Chem. Eng. Data* **2004**, 49, 675–683.
https://doi.org/10.1021/je030247m

52. B. Cabal, C. O. Ania, J. B. Parra and J. Pis, *Chemosphere.* **2009**, 76, 433–438.
https://doi.org/10.1016/j.chemosphere.2009.04.002

53. C.-F. Chang, C.-Y. Chang, K.-H. Chen, W.-T. Tsai, J.-L. Shie and Y.-H. Chen, *J. Colloid Interface Sci* **2004**, 277, 29–34.
https://doi.org/10.1016/j.jcis.2004.04.022

54. B. Pan, D. Lin, H. Mashayekhi and B. Xing, *Environ. Sci. Technol* **2008**, 42, 5480–5485.
https://doi.org/10.1021/es8001184

55. P. Lazar, F. Karlický, P. Jurečka, M. Kocman, E. Otyepková, K. Šafářová and M. Otyepka, *J. Am. Chem. Soc* **2013**, 135,

6372–6377. https://doi.org/10.1021/ja403162r

56. B. X. D. Lin, *Environ. Sci.* Technol **2008**, 42, 7254–7259. https://doi.org/10.1021/es801297u

57. M. S. I. Efremenko, *Langmuir.* **2006**, 22, 3614–3621. https://doi.org/10.1021/la052100u

58. X. W. K. Yang, L. Zhu, B. Xing, *Environ. Sci.* Technol **2006**, 40, 5804–5810. https://doi.org/10.1021/es061081n

59. W. W. K. Yang, Q. Jing, L. Zhu, *Environ. Sci.* Technol **2008**, 42, 7931–7936. https://doi.org/10.1021/es801463v

60. J. J. P. M. Sander, *Environ. Sci.* Technol **2005**, 39, 1606–1615. https://doi.org/10.1021/es049135l

61. F.-G. Klärner and T. Schrader, *Acc. Chem. Res* **2012**, 46, 967–978.

62. M. Hardouin–Lerouge, P. Hudhomme and M. Sallé, *Chem. Soc. Rev* **2011**, 40, 30–43. https://doi.org/10.1039/B915145C

63. J. Leblond and A. Petitjean, *ChemPhysChem* **2011**, 12, 1043–1051. https://doi.org/10.1002/cphc.201001050

64. C. Chen and H. Whitlock Jr, *J. Am. Chem. Soc* **1978**, 100, 4921–4922. https://doi.org/10.1021/ja00483a063

Povzetek

Modificiran grafenov oksid smo pripravili z namenom njegove uporabe kot odstranjevalca aromatskih onesnaževalcev iz vodnih raztopin. Grafenov oksid (GO) smo funkcionalizirali z 9-aminoantracenom in pripravili grafenov oksid 9-aminoantracen (GO-9-AA). Za karakterizacijo adsorbenta smo uporabili naslednje metode: infrardečo spektroskopijo (FTIR), rentgensko praškovno difrakcijo (XRD), termogravimetrično analizo (TGA), transmisijsko elektronsko mikroskopijo (TEM in ramansko spektroskopijo. Kot modelne aromatske ogljikovodike, primerne za preučevanje adsorpcije, smo uporabili naftalen (NAP), acenaftalen (ACN) in fenantren (PHN). Adsorbent GO-9-AA je bil zelo učinkovit v primeru odstranjevanja aromatskih ogljikovodikov iz vodnih raztopin. Ravnotežni podatki adsorpcijskih procesov sledijo Freundlichovemu modelu, maksimalne adsorpcijske kapacitete za preučevane aromatske ogljikovodike pa lahko podamo z zaporedjem NAP > ACN >PHN. Iz podatkov kinetične analize lahko razberemo, da je proces hiter in učinkovit in ustreza kinetičnemu modelu psevdo-drugega reda. Obroči antracena na grafenovem oksidu (GO-9-AA) so »bogati« s π elektroni in zaradi tega pospešujejo interakcijo le-tega z aromatskimi ogljikovodiki (NAP, ACN in PHN).